IOP Publishing
Superconductor Science and Technology
Supercond. Sci. Technol. **30** (2017) 085008 (12pp)
https://doi.org/10.1088/1361-6668/aa76a2

Simulation studies of mechanical stresses in REBaCuO superconducting ring bulks with infinite and finite height reinforced by metal ring during field-cooled magnetization

H Fujishiro[1,5], M D Ainslie[2], K Takahashi[1], T Naito[1], Y Yanagi[3], Y Itoh[3] and T Nakamura[4]

[1] Department of Physical Science and Materials Engineering, Faculty of Science and Engineering, Iwate University, 4-3-5 Ueda, Morioka 020-8551, Japan
[2] Bulk Superconductivity Group, Department of Engineering, University of Cambridge, Trumpington Street, Cambridge CB2 1PZ, United Kingdom
[3] IMRA Material R&D Co., Ltd, 2-1 Asahi-machi, Kariya 448-0032, Japan
[4] RIKEN, 2-1 Hirosawa, Wako 351-0198, Japan

E-mail: fujishiro@iwate-u.ac.jp

Received 7 April 2017, revised 19 May 2017
Accepted for publication 2 June 2017
Published 10 July 2017

Abstract

We have performed the numerical simulation of mechanical stresses (hoop stress, σ_θ and radial stress, σ_r) in REBaCuO ring bulks with an infinite and finite height reinforced by metal (aluminum alloy or stainless steel) ring during field-cooled magnetization (FCM) using a solenoid coil with an infinite and finite height. The superconducting characteristics of the bulk material were assumed to follow Bean's critical state model. The electromagnetic hoop stress, σ_θ^{FCM}, of the finite height ring bulk during FCM using the infinite coil was larger than that for the infinite ring bulk, and the time step dependence of σ_θ^{FCM} was clearly different in each case. The σ_θ^{FCM} value was reduced by the reinforcement by the metal ring, and the stainless steel ring was more effective than the aluminum alloy ring. The σ_θ^{FCM} value of the finite ring bulk magnetized using the finite coil was slightly reduced, compared to magnetization using the infinite coil. The thermal hoop stress, σ_θ^{cool}, which occurs in the ring bulk when cooling down to operating temperature due to the difference of thermal contraction coefficient between ring bulk and metal ring, was also estimated. The compressive, σ_θ^{cool}, was reduced comparatively at the uppermost surface of the ring bulk because of the larger thermal contraction of the metal ring along the axial direction. The actual total hoop stress, $\sigma_\theta (=\sigma_\theta^{FCM} + \sigma_\theta^{cool})$ was analyzed for the finite ring bulk reinforced by the metal ring during FCM and the possibility of mechanical fracture due to this hoop stress is also discussed.

Keywords: mechanical properties, field-cooled magnetization, REBaCuO bulk, metal ring reinforcement, hoop stress, trapped field

(Some figures may appear in colour only in the online journal)

1. Introduction

One of the most promising practical applications of superconducting bulks such as REBaCuO (RE: rare earth element or Y) and MgB_2 is to realize a strong trapped field magnet (TFM), which continues to attract increasing attention because of improvements in superconducting material properties and sample size. When the superconducting bulk is magnetized by field-cooled magnetization (FCM), the magnetic flux is trapped at pinning centers and an induced

[5] Author to whom any correspondence should be addressed.

persistent current flows concentrically inside the bulk, in which a current-field interaction, that is, a Lorentz force exists in the bulk. At present, REBaCuO disk bulks can trap magnetic fields over 17 T by the mechanical reinforcement using glass fiber reinforced epoxy resin or shrink-fit steel to reduce the electromagnetic hoop stress [1, 2]. At such high fields, the performance of the bulk superconductor as a magnet is limited not by its superconducting properties, but its mechanical properties [1]. Recently, annular REBaCuO bulks with a larger bore have been used for a compact and cryogen-free nuclear magnetic resonance (NMR) spectrometer and a magnetic resonance imaging (MRI) apparatus, in which a uniform trapped field as high as 4.7 T can be achieved in the hollow space of the cylindrical bulks [3–7]. To enhance the resolution of the NMR signal, it is necessary to achieve a higher trapped field in the REBaCuO ring bulk. During the magnetizing process for superconducting bulks, the mechanical strength of the bulk material must be considered to avoid fracture, because the REBaCuO bulk is a brittle ceramic material and has a low mechanical strength of 30–100 MPa, which is strongly related to the fabrication process [8, 9]. The addition of the Ag and the reduction of voids in the bulk during the growth process are also effective to increase in the mechanical strength [10]. The ring bulk, in particular, suffers from higher mechanical stress than the disk bulk because of the concentration of the hoop stress at the innermost periphery [11].

Ren *et al* reported the experimental results and analytical solutions of the mechanical stresses of the TFM using the expanded theory for the infinite bulk cylinder [12]. Johansen *et al* presented analytical solutions of the flux-pinning-induced stress and strain distributions in the infinite bulk cylinder and ring and a thin disk, including the magnetostriction during FCM and zero-FCM [13–15]. These papers were based on Bean's critical state model for a *c*-axis oriented, infinite superconducting cylinder, in which the critical current density, J_c, is independent of the magnetic field. We have performed numerical simulations of the hoop and radial stresses during the pulsed field magnetization (PFM) of a GdBaCuO ring bulk reinforced by an aluminum alloy ring using a finite element method (FEM) [11], in which the height of the ring bulk was assumed to be infinite and Bean's model was assumed. The compressive and tensile hoop stresses were, respectively, concentrated at the innermost peripheral edge of the infinite ring bulk during the ascending and descending stages of the PFM process, together with the compressive stress due to the thermal contraction by cooling. Huang *et al* investigated the magnetostriction of superconducting cylinders and rings with finite height by FEM [16], in which Bean's model and a uniform applied field using an infinite magnetizing solenoid coil were assumed. They concluded that the mechanical response of the finite height bulk is similar to that of an infinitely long bulk, but there is also a difference due to boundary and demagnetization effects. However, there has been no investigation of mechanical stresses for the finite ring bulk magnetized by a solenoid coil of infinite and finite height in previous studies, and no comparison has been made to the infinite height bulk. Furthermore, there have been no numerical simulations of the reinforcement effect of the metal ring fitting on the mechanical stresses in superconducting bulk rings and disks during FCM and cooling, except for the relevant work by Johansen *et al* [17].

In this paper, we perform numerical simulations of the electromagnetic stresses (hoop stress, $\sigma_\theta^{\,\mathrm{FCM}}$, and radial stress, $\sigma_r^{\,\mathrm{FCM}}$), together with the superconducting characteristics (trapped field, B_z, and induced persistent current density, J_θ) in the REBaCuO ring bulk of infinite and finite height, and reinforced by an aluminum alloy ring, during FCM using infinite and finite solenoid magnetizing coils. The influences of the bulk height and the coil height on the mechanical stresses are investigated. We also investigate the reinforcement effect of a stainless steel ring on the hoop stress, which is a typical material for mechanical reinforcement [1]. The relationship between the mechanical stresses and the bulk fracture during the FCM process is discussed, under the thermal compressive stress, $\sigma_\theta^{\,\mathrm{cool}}$, which occurs in the ring bulk when cooling, due to the difference of thermal contraction coefficient between ring bulk and metal ring.

2. Numerical simulation framework

Based on our experimental setup for the FCM procedure [18], we prepared the following framework of three-dimensional numerical simulation. Schematic views of three types of numerical models are presented in figure 1. The ring bulk with infinite height (64 mm outer diameter (O.D.) and 40 mm inner diameter (I.D.)) reinforced by the metal ring (aluminum alloy) of 5 mm in thickness was magnetized by FCM using an infinite solenoid coil (150 mm O.D., 100 mm I.D. and infinite height), as shown in figure 1(a). We abbreviate this setup as 'case A'. The REBaCuO ring bulk with a finite height of 20 mm was mounted in the metal ring with the same height as the ring bulk, as shown in figure 1(b), which was magnetized by the infinite solenoid coil. We abbreviate this setup as 'case B'. The same finite ring bulk with the metal (aluminum alloy or stainless steel) ring was magnetized by a finite solenoid coil (150 mm O.D., 100 mm I.D. and 100 mm height), as shown in figure 1(c). We abbreviate this setup as 'case C'. Physical phenomena in the simulation during FCM are described using electromagnetic equation [19–21], in which the temperature of the REBaCuO bulk is assumed to be constant at $T_s = 50$ K during FCM for simplicity, because the actual temperature rise during FCM from 6.3 T was as low as $\sim$2 K under a descending speed of 0.1 T min^{-1} [22]. The power-n model ($n = 100$) was used to describe the nonlinear E–J characteristic of the superconducting bulk;

$$E = E_c\left(\frac{J}{J_c}\right)^n, \tag{1}$$

where E_c ($=10^{-4}$ V m^{-1}) is the reference electric field and J_c ($=4.8 \times 10^8$ A m^{-2}) is the critical current density under zero field, which is a typical J_c value at $T_s = 50$ K for the REBaCuO bulk [7]. J_c is assumed to be independent of applied magnetic field [7]. For an 'infinite disk bulk' with the same O.D., not the 'infinite ring bulk', the fully magnetized trapped field is estimated to be $B_z^* = \mu_0 J_c R = 19.30$ T (R: radius of the disk bulk) by

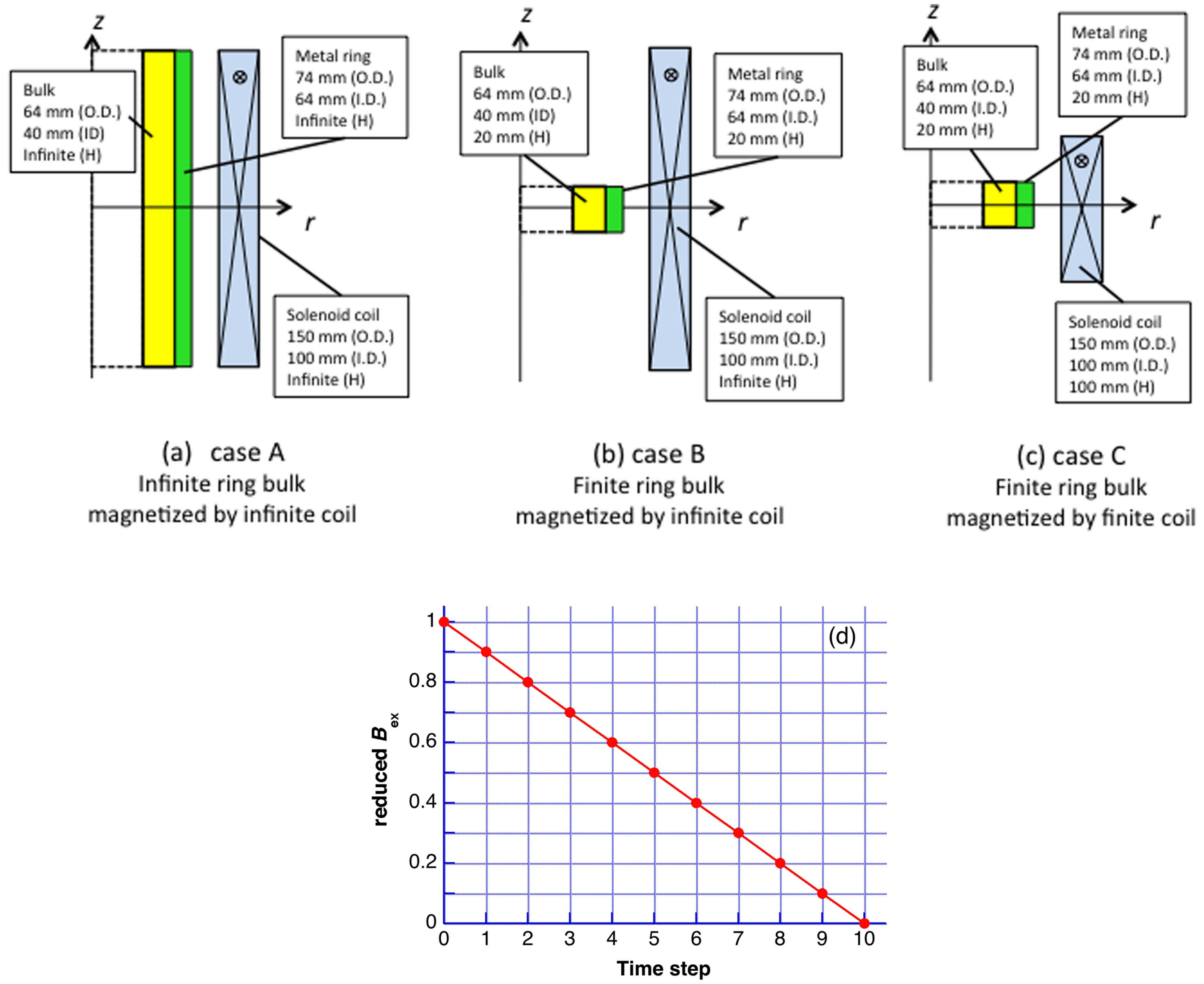

Figure 1. Three types of models for the numerical simulation during FCM for the (a) infinite ring bulk magnetized by solenoid coil with infinite height (‘case A’), (b) finite ring bulk magnetized by solenoid coil with infinite height (‘case B’) and (c) finite ring bulk magnetized by solenoid coil with finite height (‘case C’). For each case, the ring bulk was reinforced by a metal ring 5 mm in thickness and with the same height as the ring bulk. The dimensions of the ring bulk, metal ring and the magnetizing coil are also shown. (d) Time step of the reducing applied field during FCM from B_{ex}, in which the applied field is linearly decreased to zero in ten steps.

Bean’s model. We confirmed that the larger n value than 80 and constant J_c values realized the approximate Bean’s model. In the simulation process of FCM, a magnetic field of $B_{ex} = 4.7$ T or 9.4 T was applied above the critical temperature, T_c (= 92 K), and then the ring bulk was cooled to $T_s = 50$ K. Thereafter, the magnitude of the magnetic field was monotonically decreased from B_{ex} to zero in ten steps, as shown in figure 1(d). Note that the magnetic field of $B_{ex} = 4.7$ T and 9.4 T corresponds to ^{1}H resonance frequency of 200 and 400 MHz in the NMR spectrometer, respectively.

In an isotropic material, Hooke’s law is established, in which the stress is linearly proportional to the strain. For simplicity, the REBaCuO bulk is assumed to be isotropic and homogeneous. The relation is expressed using the stress tensor σ_{ij} and strain tensor, e_{ij}, in the following,

$$\sigma_{ij} = \lambda \cdot e_{kk} \cdot \delta_{ij} + 2G \cdot e_{ij}, \tag{2}$$

$$\lambda = \frac{E \cdot \nu}{(1+\nu)(1-2\nu)}, \tag{3}$$

$$G = \frac{E}{2(1+\nu)}, \tag{4}$$

where λ and G represent the Lame’s constants, δ_{ij} is the Kronecker delta function, E is the Young’s modulus, and ν is the Poisson ratio. The electromagnetic hoop stress, $\sigma_\theta^{\text{FCM}}$, and the electromagnetic radial stress, σ_r^{FCM}, were calculated for each step of FCM based on the axisymmetric coordinate system, in which $\sigma_\theta^{\text{FCM}}$ acts circumferentially on each end

Table 1. Mechanical properties used in the numerical simulation [11].

	E (Pa)	ν	α (K^{-1})
REBaCuO bulk	1.0e11	0.33	5.2e-6
Al alloy ring	7.8e10	0.34	1.48e-5
SUS304 ring	1.93e11	0.28	1.27e-5

(E: Young's modulus, ν: Poisson ratio, α: thermal contraction coefficient.)

face of the meshed element and σ_r^{FCM} acts radially on the inner and outer curved surfaces of the element [12, 13]. The thermal hoop stress, σ_θ^{cool}, by cooling from 300 to 50 K was also calculated, which was generated by the difference of the thermal contraction coefficient, α, between the superconducting bulk and the metal ring material. The mechanical parameters (E, ν, and thermal contraction coefficient, α) of the bulk and ring materials used in the elastic simulation are summarized in table 1 [11]. Commercial software, Photo-Eddy (Photon Ltd, Japan) was used for the analysis of the distributions of magnetic field, B_z, along z-direction and the induced persistent current density, J_θ, along the circumferential direction during FCM. The σ_θ^{FCM} and σ_r^{FCM} values were calculated for each step by Photo-ELAS (Photon Ltd, Japan) using the nodal force at each node calculated by Photo-Eddy. In a half model ($z \geqslant 0$), the ring bulk with metal ring was equally divided into 36 elements along the circumferential (θ) direction and 17 elements along the r-direction and ten elements along the z-direction.

3. Results and discussion

3.1. Time step dependence of trapped field, B_z, and induced current density, J_θ

Figures 2(a) and (b), respectively, show the time step dependence of the cross-section of the trapped field along the z-direction, B_z, and the induced superconducting current density in the θ-direction, J_θ, for the 'case A' (infinite bulk magnetized by infinite coil). In figure 2(a), the external magnetic field decreased step by step without a field slope due to the infinite length of magnetizing solenoid coil. In the ring bulk periphery, the penetrated magnetic field monotonically decreases with increasing time step and has a constant field slope, which is equivalent to a constant critical current density, J_c, based on Bean's model. The J_θ, which is equal to J_c, flows only in the outer region of the ring bulk ($24 \leqslant r \leqslant 32$ mm) up to the final step, as shown in figure 2(b), because of the lower applied field, compared to B_z^* that results in full magnetization. As a result, the magnetic field, B_z, in the hole at $r \leqslant 20$ mm is the same as the applied field, $B_{ex} = 4.7$ T.

Figures 2(c) and (d), respectively, show similar plots of B_z and J_θ at $z = 0$ for 'case B' (finite bulk magnetized by infinite coil). It should be noted that, in figure 2(c), the initial B_z profile at step 0 is independent of r because of the infinite magnetizing coil. The external magnetic field decreased step by step with a field slope due to the existence of superconducting bulk, despite using the infinite solenoid coil. In the ring bulk region ($20 \leqslant r \leqslant 32$ mm), the induced persistent current flows only in the periphery of the ring bulk at the early step up to the 6th step as shown in figure 2(d). The current flowing region moves into the inside and the persistent current flows fully in the ring bulk after the sixth step due to the reduction of the external field. As a result, the trapped field at the center in the hole ($r = z = 0$) decreases step by step, and the final trapped magnetic field reaches 2.70 T. It should be noted that the electromagnetic properties for the finite ring bulk drastically change, compared to those for the infinite ring bulk using the same infinite magnetizing coil, which can be clearly observed for the first time.

Figures 2(e) and (f) show similar plots of B_z and J_θ, respectively, at $z = 0$ for the 'case C' (finite bulk magnetized by finite coil). The B_z and J_θ profiles are nearly the same as those for the 'case B' shown in figures 2(c) and (d), except for the initial $B_z(r)$ profile at step 0 with a slight gradient because of the use of the finite coil. The trapped field decreases step by step, and the final magnetic field at the center in the hole of the ring bulk ($r = z = 0$) reaches 2.70 T, which was the same as that for 'case B', because a persistent current with the same J_c flows over the entire cross-section of the ring bulk (as shown in figure 2(f), which is the same result as 'case B' shown in figure 2(d)). The $B_z(r)$ profile at the bulk surface ($z = 9.9$ mm) is also shown in figure 2(e), for which the magnitude of B_z at $z = 9.9$ mm is smaller than that at $z = 0$ because of the edge effect of the finite ring bulk. There is little influence of the coil height on the electromagnetic properties for the finite ring bulk, as observed when comparing figures 2(c) and (e) and figures 2(d) and (f). Because the solenoid coil height in 'case C (100 mm)' is much higher than the bulk height (20 mm).

Figure 3 shows the contour maps of the trapped field, B_z, in the ring bulk at the (a) fourth step for 'case A', (b) 2nd step for 'case C,' and (c) fourth step for 'case C'. The contour maps of the persistent current density, J_θ, for each case are also shown in the lower panels from (d) to (f). The B_z profile of the fourth step in 'case A' shown in figure 3(a), which is the infinite bulk magnetized by the infinite coil, is axisymmetric along the z-direction due to the axisymmetric J_θ profile shown in figure 3(d). On the other hand, the B_z profile of the 2nd step in 'case C' shown in figure 3(b), which is finite bulk magnetized by finite coil, is rounded around the surface of the finite bulk, in which the persistent current similar to J_c flows even around the surface region as shown in the red region in figure 3(e). The region of the persistent current increases with increasing the time step, such as the fourth step as shown in figure 3(f) and, as a result, the B_z profile clearly becomes rounded at the fourth step shown in figure 3(c).

Figure 4 shows the time step dependence of the trapped field, B_z, at the center ($r = z = 0$) in the hole of the infinite and finite ring bulks during FCM from $B_{ex} = 4.7$ or 9.4 T for all three cases. For 'case A', the B_z value of the infinite bulk maintains 9.4 T up to the seventh step for $B_{ex} = 9.4$ T, at which the induced persistent current with the same value to J_c flows in the whole part of the bulk, and then B_z decreases with increasing time steps. The final B_z value was 7.5 T. For

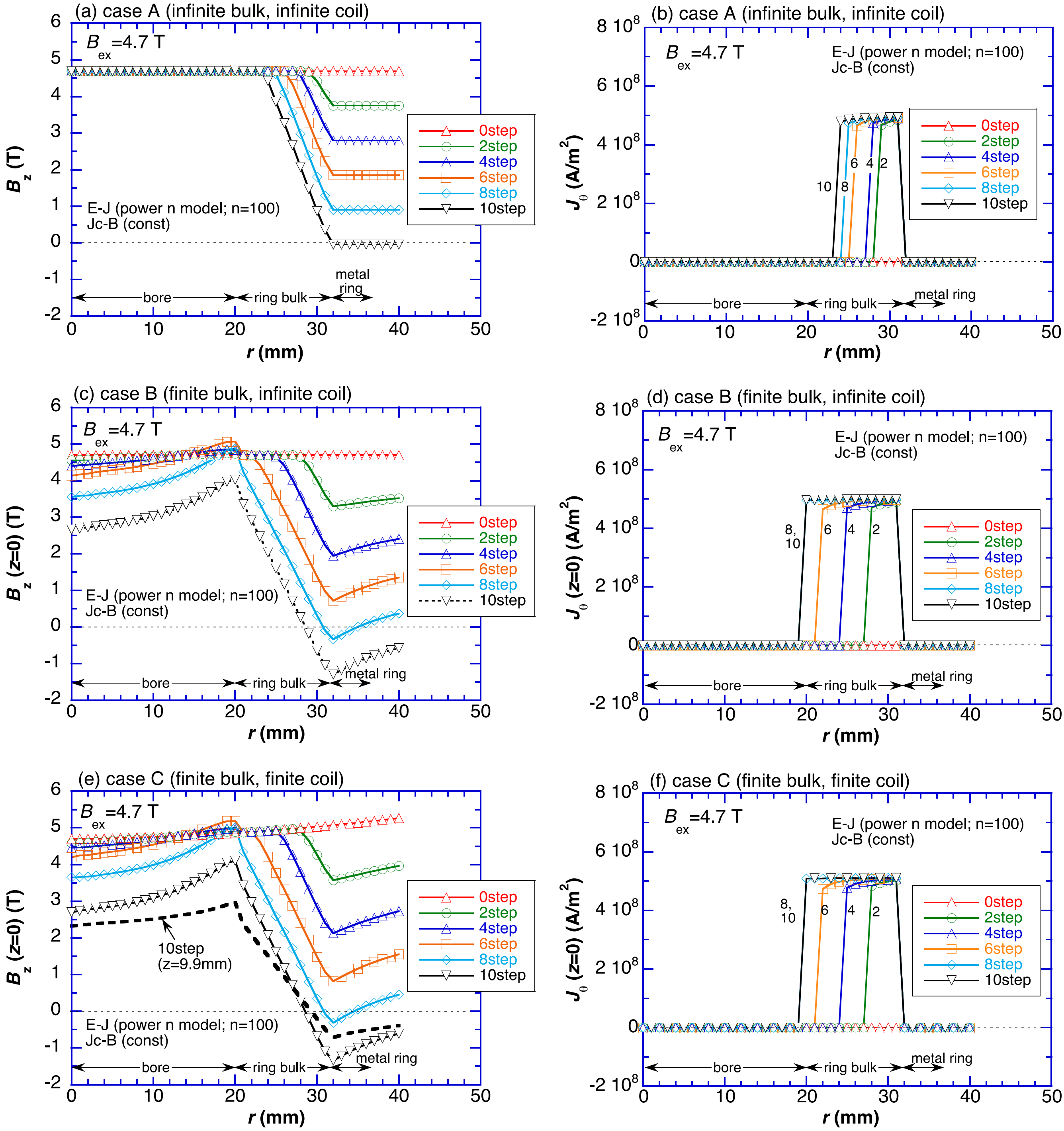

Figure 2. Time step dependence of the cross-sectional plots of the trapped field, $B_z(r)$, along the z-direction for (a) 'case A' (infinite bulk magnetized by infinite coil), (c) 'case B' (finite bulk magnetized by infinite coil), and (e) 'case C' (finite bulk magnetized by finite coil) during FCM from $B_{ex} = 4.7$ T. The time step dependence of the cross-sectional plots of the induced superconducting current density, $J_\theta(r)$, in the θ-direction for each case is shown in (b), (d) and (f).

$B_{ex} = 4.7$ T in 'case A', the B_z value of the infinite bulk maintains 4.7 T up to the final step. These results for 'case A' can be reproduced using analytical equations based on Bean's model [21]. On the other hand, for 'case B' and 'case C' for the finite ring bulk at $B_{ex} = 9.4$ T, B_z gradually decreased up to the third step, at which the region of current flow reaches the central part of the ring bulk. Thereafter, B_z more rapidly reduces to the final step to $B_z = 2.75$ T, at which the $J_\theta = J_c$ flows across the whole bulk cross-section. For $B_{ex} = 4.7$ T, B_z gradually decreased up to the sixth step and then decreased more rapidly to the final value of $B_z = 2.74$ T, which is nearly the same as that for $B_{ex} = 9.4$ T. It should be noted that the time step dependence of the B_z value for the finite bulk can be obtained only by FEM, although the B_z value is analytically

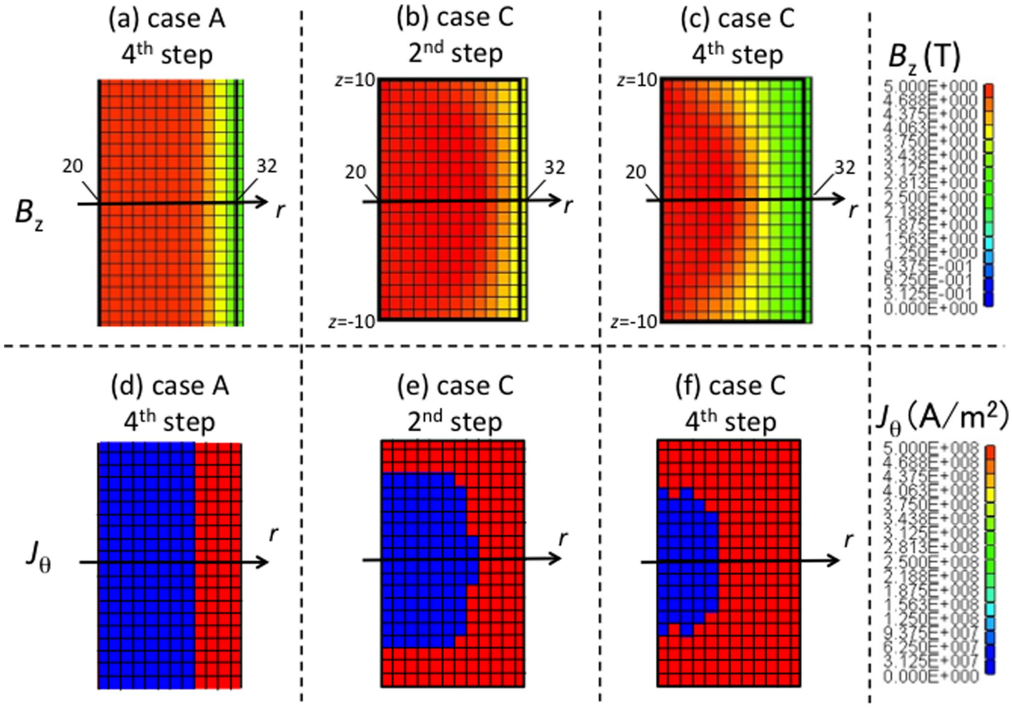

Figure 3. Contour maps of the trapped field, B_z, in the ring bulk at the (a) fourth step in 'case A', (b) second step in 'case C' and (b) fourth step in 'case C' during FCM from 4.7 T. The cross sections of the persistent current density, J_θ, for each case are also shown in the lower panels from (d) to (f), in which the persistent current similar to J_c ($= 4.8 \times 10^8$ A m^{-2}) flows in the 'red region' perpendicular to the paper space.

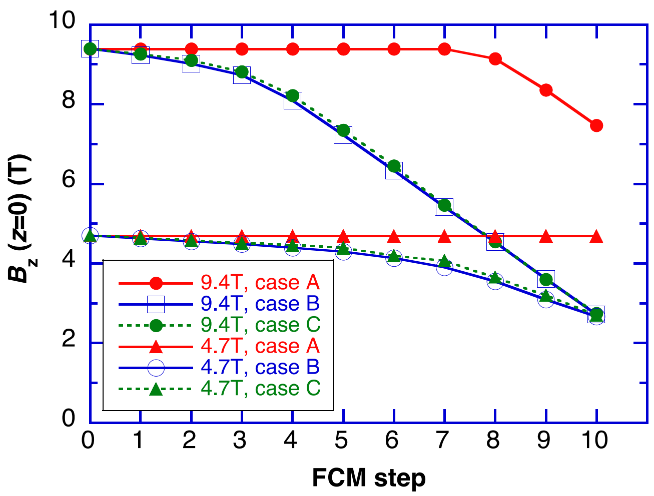

Figure 4. Time step dependence of the trapped field, B_z, at the center ($r = z = 0$) of the hole for three cases during FCM from $B_{ex} = 4.7$ and 9.4 T.

calculated for the infinite bulk. In this way, the time step dependence of the trapped field and induced persistent current density in the finite and infinite ring bulks can be estimated during the FCM process using the FEM method.

3.2. Mechanical stresses during FCM

3.2.1. Electromagnetic hoop stress, σ_θ^{FCM}, and radial stress, σ_r^{FCM} for the finite and infinite ring bulks without cooling. To confirm the reliability of the present numerical simulation for the mechanical stresses, we calculated the r dependences of the electromagnetic hoop stress, σ_θ^{FCM}, and electromagnetic radial stress, σ_r^{FCM}, for infinite ring bulk during FCM, in which Ren's analytical equations for the infinite disk bulk [12] were modified for the infinite ring-shaped bulk [23]. Figure 5 shows the comparison between the numerical simulation results and analytical ones of the cross-sectional plots of σ_θ^{FCM} and σ_r^{FCM} for the 'case A' without any reinforcement by metal ring at the final step of FCM from $B_{ex} = 4.7$ T. The obtained values by the present FEM method showed an excellent agreement with those by the analytical equations, which could give the exact solution.

Figures 6(a) and (b) present the time step dependences of the cross-sectional plots of the electromagnetic hoop stress, σ_θ^{FCM}, and the electromagnetic radial stress, σ_r^{FCM}, respectively, in the infinite bulk reinforced by an aluminum alloy ring during FCM from $B_{ex} = 4.7$ T for 'case A'. In this subsection, we assume that there is no thermal stress in the bulk. In figure 6(a), the electromagnetic hoop stress, σ_θ^{FCM}, increases with increasing FCM time step, takes a maximum of 23 MPa at the innermost periphery edge of the ring bulk ($r = 20$ mm) at the final step. At each time step, the σ_θ^{FCM} value decreases with increasing r, but steeply drops at the interface ($r = 32$ mm) between bulk and aluminum alloy ring, which results from the smaller Young's modulus, E, of the aluminum alloy ring, as shown in table 1. The time step and the r dependence of σ_r^{FCM} shown in figure 6(b) are clearly different to the σ_θ^{FCM} behaviors; the magnitude of σ_r^{FCM} is fairly smaller and the time step dependence is not monotonous.

Figures 6(c) and (d) show similar plots of σ_θ^{FCM} and σ_r^{FCM}, respectively, at $z = 0$ in the finite bulk reinforced by an aluminum alloy ring for 'case B' (magnetized by infinite

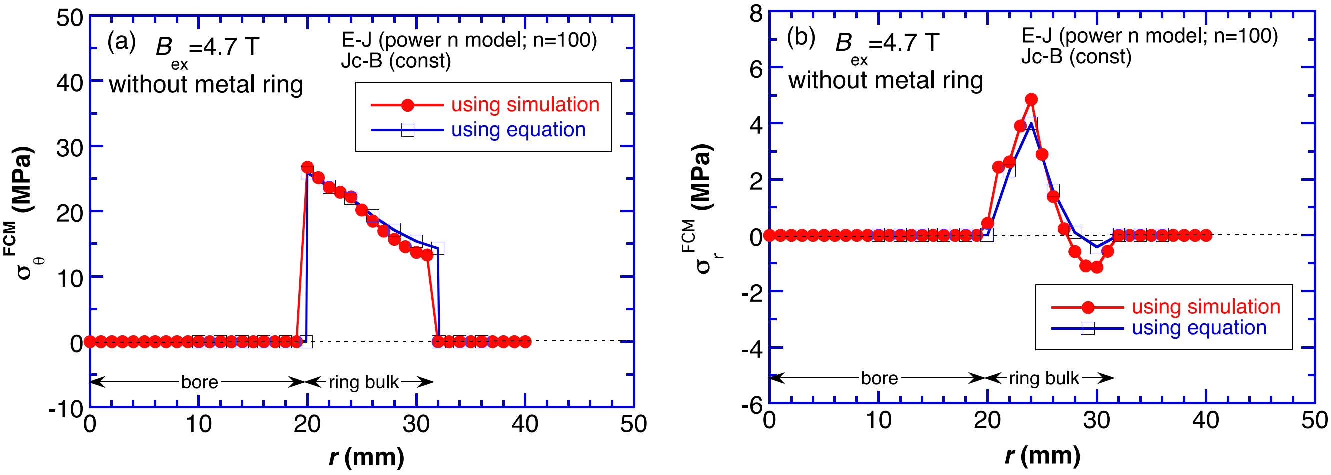

Figure 5. The comparison between the numerical simulation results and analytical ones of the cross-sectional plots of (a) electromagnetic hoop stress, σ_θ^{FCM}, and (b) electromagnetic radial stress, σ_r^{FCM}, for the infinite ring bulk without any reinforcement, magnetized by infinite magnetizing coil ('case A') during FCM from $B_{ex} = 4.7$ T.

solenoid coil). The time step dependence of σ_θ^{FCM} and σ_r^{FCM} is clearly different to 'case A'. The σ_θ^{FCM} value increases with increasing time steps, takes a maximum of 37 MPa at the innermost periphery of the ring bulk at the sixth step, which is about 1.6 times as large as the maximum value in 'case A', and then decreases with increasing time steps. This difference results from the Lorentz force, $F = J_\theta \times B$, that exists over a larger region of the finite ring bulk, where the induced persistent current, J_θ, flows over a wider area of the finite ring bulk cross-section than for the infinite ring bulk. The time step dependence of the σ_r^{FCM} behavior is also different to that of the infinite bulk in 'case A'. It should be noted that the mechanical stresses for the finite ring bulk drastically change, compared to those for the infinite ring bulk for the infinite magnetizing coil, which can be clearly observed for the first time.

Figures 6(e) and (f) show similar plots of σ_θ^{FCM} and σ_r^{FCM}, respectively, at $z = 0$ in the finite ring bulk reinforced by an aluminum alloy ring for 'case C' (magnetized by the finite solenoid coil). The time step dependence of the σ_θ^{FCM} and σ_r^{FCM} closely resembles to that for 'case B' with a very slight increase in magnitude. These results suggest that the influence of the magnetizing coil height on the electromagnetic stresses for the finite ring bulk is not so large from figures 6(c)–(f).

Figures 7(a) and (b) show the cross-sectional plots of the electromagnetic hoop stress, σ_θ^{FCM}, and the electromagnetic radial stress, σ_r^{FCM}, respectively, in the finite ring bulk reinforced by an aluminum alloy ring at the sixth step during FCM from $B_{ex} = 4.7$ T for 'case C', at which the σ_θ^{FCM} takes a maximum. The σ_θ^{FCM} is axisymmetric and is independent of the z-position due to the uniform flow of a persistent current with the same J_c. On the other hand, σ_r^{FCM} is axisymmetric, but does depend on the z-position, which is about one order of magnitude smaller than σ_θ^{FCM}. These results suggest that the bulk fracture might start from innermost periphery of the ring bulk by means of the electromagnetic hoop stress and that the electromagnetic radial stress has little influence on the bulk fracture.

Figure 8(a) shows the time step dependence of the maximum electromagnetic hoop stress, σ_θ^{FCM}(max), for the ring bulks with (w/) and without (w/o) the aluminum alloy ring during FCM for each case from $B_{ex} = 4.7$ T. In all cases, σ_θ^{FCM}(max) initially increases with increasing time step, takes a maximum, and then decreases, and the location of σ_θ^{FCM}(max) occurs at the innermost surface of the ring bulk. However, the time step at which the σ_θ^{FCM}(max) value is achieved, and the maximum σ_θ^{FCM}(max) value change depending on the height of the ring bulk; σ_θ^{FCM}(max) takes a maximum at the tenth (final) step for the infinite bulk, but for the finite bulk, it takes a maximum at the sixth step and is larger than that for the infinite bulk. The σ_θ^{FCM} value decreased about 20% by the reinforcement with the aluminum alloy ring in all cases, which results from the relative compressive stress from the aluminum alloy ring, because the aluminum alloy ring restricts the expansion of the ring bulk due to the Lorentz force during FCM.

Figure 8(b) shows the same plots during FCM for each case from $B_{ex} = 9.4$ T. The maximum σ_θ^{FCM} value and the time step at which this maximum takes place are different to that of the 4.7 T case. The maximum σ_θ^{FCM} value for 'case C', which takes place at the third (or fourth) step, increased to 100 MPa, which is larger than that for the infinite ring bulk, which takes a maximum at the eighth step. These results suggest that the σ_θ^{FCM}(max) value for the infinite ring bulk, which can be calculated by analytical equations [23], might be underestimated, compared to that of the actual finite ring bulk. Therefore, estimation of the hoop stress must be performed for the actual finite bulk reinforced by the metal ring using numerical simulations to avoid the mechanical fracture of the bulk during FCM.

3.2.2. Influence of thermal contraction on the hoop stress in the ring bulk reinforced by metal (aluminum alloy or SUS) ring. In this subsection, we investigate the influence of thermal contraction on the hoop stress, σ_θ^{cool}, in the ring bulk reinforced by a metal ring. Figure 9(a) shows the radius (r) dependence of the thermal hoop stress, σ_θ^{cool}, in the finite

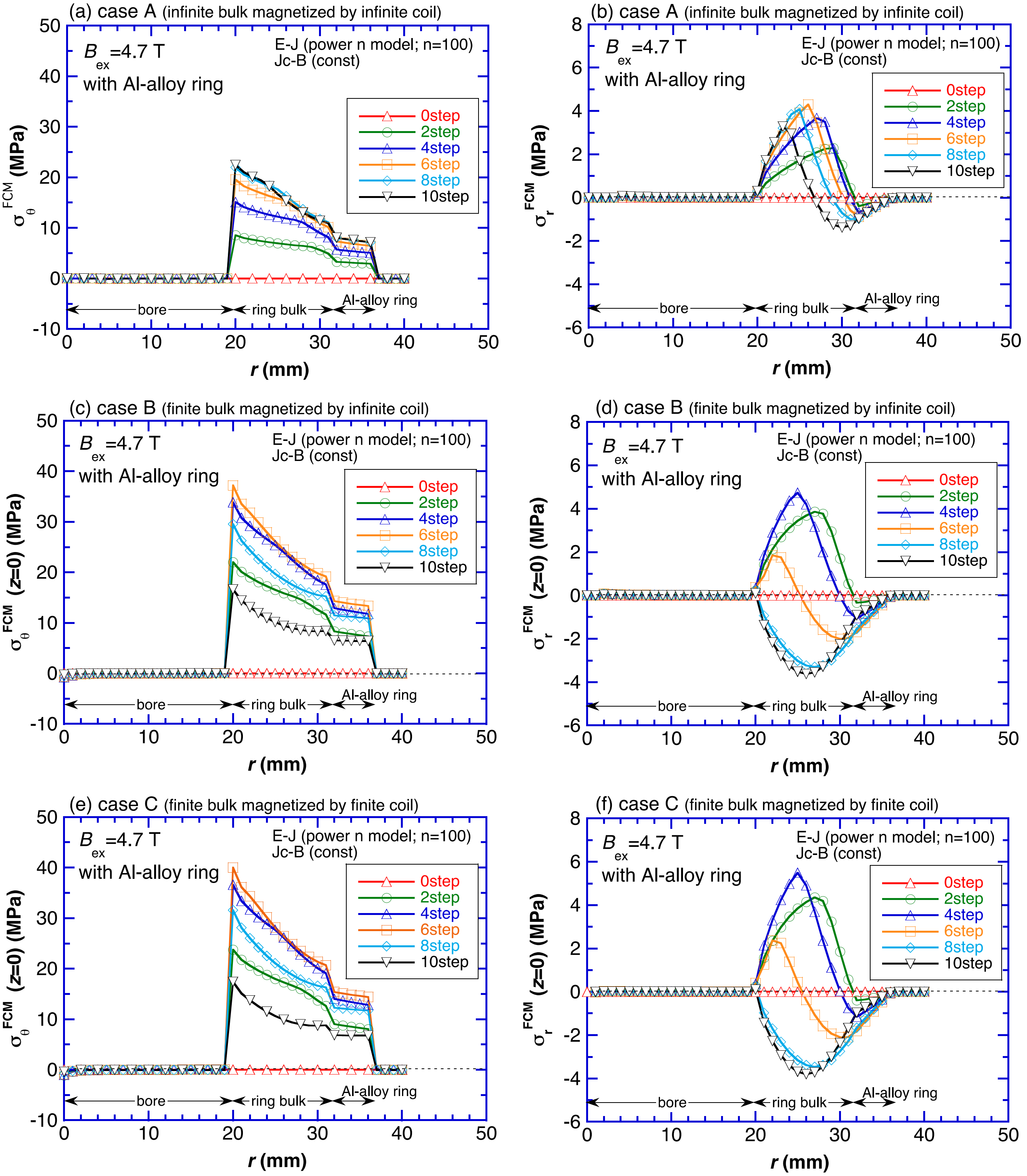

Figure 6. Time step dependence of the cross-sectional plots of (a) electromagnetic hoop stress, $\sigma_\theta{}^{FCM}$, and (b) electromagnetic radial stress, $\sigma_r{}^{FCM}$, for the infinite ring bulk magnetized by infinite coil ('case A') during FCM from $B_{ex} = 4.7$ T. (c) and (d) show similar $\sigma_\theta{}^{FCM}$ and $\sigma_r{}^{FCM}$ plots for the finite ring bulk magnetized by the infinite coil ('case B'), and (e) and (f) show similar plots for the finite ring bulk magnetized by the finite coil ('case C'). In all cases, the ring bulk was reinforced by an aluminum alloy ring.

ring bulk reinforced by an aluminum alloy ring at various z-positions under the cooling from 300 to 50 K without FCM. In the ring bulk region ($20 \leqslant r \leqslant 32$ mm), a thermally compressive stress ($\sigma_\theta < 0$) is applied to the ring bulk, and a tensile stress ($\sigma_\theta > 0$) is applied to the aluminum alloy ring ($32 \leqslant r \leqslant 37$ mm), because the thermal contraction coefficient, α, of the aluminum alloy is about three times larger than that of the superconducting bulk, as shown in

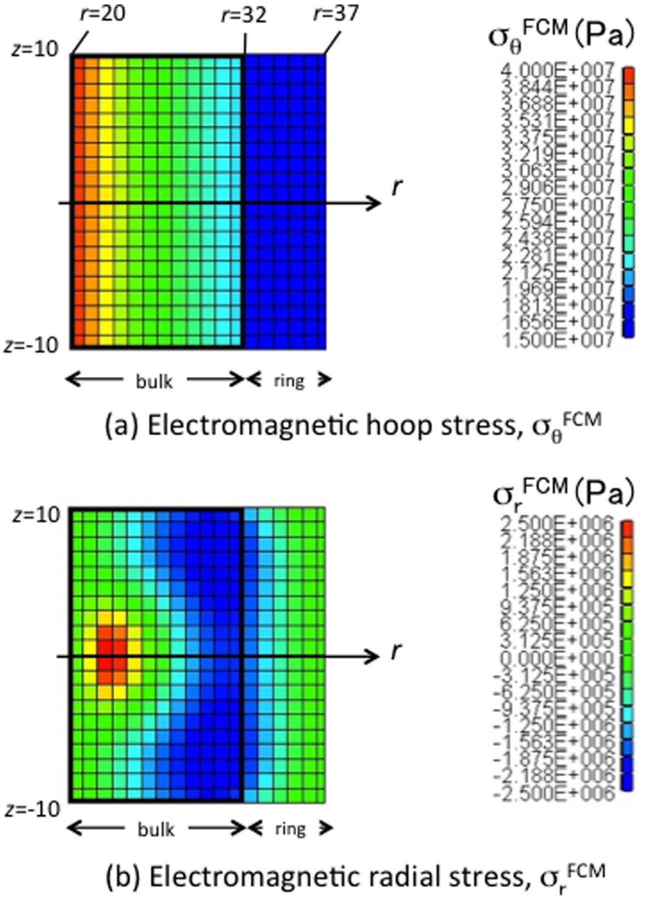

Figure 7. Contour maps of (a) electromagnetic hoop stress, $\sigma_\theta^{\,\mathrm{FCM}}$, and (b) electromagnetic radial stress, $\sigma_r^{\,\mathrm{FCM}}$, at the sixth step during FCM from $B_{\mathrm{ex}} = 4.7$ T in 'case C' (finite bulk magnetized by the finite coil).

table 1. The compressive stress for the bulk at the center ($z = 0$) is -56 MPa at $r = 20$ mm and -115 MPa at $r = 31$ mm, and gradually decreases with increasing z. It is surprising that the $\sigma_\theta^{\,\mathrm{cool}}$ value of the ring bulk surface ($z = 9.9$ mm) changed to positive (tensile stress) at the bulk periphery ($r > 27$ mm). Figure 9(b) shows the contour map of the displacement, dz, along the z-direction in the ring bulk during the cooling. Because of the larger α value of the aluminum alloy compared to the bulk, the aluminum alloy ring shrinks along both z- and r-directions. The ring bulk was fastened along the r-direction and, at the same time, the periphery region of the ring bulk was pulled toward $z = 0$. As a result, the compressive hoop stress around the bulk periphery became weak and changes to positive. Figure 9(c) shows the contour map of the displacement, dr, along the r-direction in the ring bulk during the cooling. The magnitude of the thermal shrink at the bulk surface ($z = \pm 10$ mm) is larger than that at the bulk center ($z = 0$), which suggests that the surface region of the ring bulk is expanded like a trumpet. Note that there is no mechanical stress of thermal origin in the ring bulk during cooling, if the ring bulk is not reinforced by a metal ring.

In the actual FCM process, both the thermal and mechanical stress must be considered from both the cooling process and the FCM process. Figure 10(a) shows the radius (r) dependence of the maximum $\sigma_\theta (= \sigma_\theta^{\mathrm{FCM}} + \sigma_\theta^{\mathrm{cool}})$ value at the 4th step at various z-positions in the finite ring bulk reinforced by an aluminum alloy ring, under both the FCM process ($\sigma_\theta^{\,\mathrm{FCM}}$) of $B_{\mathrm{ex}} = 9.4$ T ('case C') and the cooling process ($\sigma_\theta^{\,\mathrm{cool}}$) from 300 to 50 K. The σ_θ value increased positively in the ring bulk by the superposition, and was $+50$ MPa at $r = 20$ mm and $+95$ MPa at $r = 31$ mm and at $z = 9.9$ mm (near the top surface of the ring bulk). These results suggest that the ring bulk might be broken by the larger electromagnetic hoop stress during the actual FCM process from 9.4 T. Figure 10(b) shows the contour map of the maximum $\sigma_\theta (= \sigma_\theta^{\mathrm{FCM}} + \sigma_\theta^{\mathrm{cool}})$ in the finite bulk at the 4th step from 9.4 T ('case C') under cooling from 300 to 50 K. The σ_θ distribution can be seen in the ring bulk and a large positive hoop stress exists at the surface of the bulk periphery.

Figure 11(a) shows the r dependence of the $\sigma_\theta^{\,\mathrm{cool}}$ value in the finite ring bulk reinforced by a SUS ring at various z-positions under cooling from 300 to 50 K without FCM. The maximum compressive $\sigma_\theta^{\,\mathrm{cool}}$ value at the center ($z = 0$) is -91 MPa at $r = 20$ mm and -140 MPa at $r = 31$ mm, which is larger than that for the ring bulk reinforced by the aluminum alloy ring (figure 9(a)), and gradually decreases with increasing z. The larger compressive $\sigma_\theta^{\,\mathrm{cool}}$ value in the ring bulk reinforced by the SUS ring results from the larger Young's modulus, E of the SUS ring, compared to that of the aluminum alloy ring, in spite of smaller thermal contraction coefficient, α, of the SUS ring. These results suggest that the ring bulk could actually be broken during only cooling, because the REBaCuO bulk has a lower mechanical strength of $+30 \sim +100$ MPa [8, 9]. Figure 11(b) presents the time step dependence of the electromagnetic hoop stress, $\sigma_\theta^{\,\mathrm{FCM}}$, for the finite ring bulk reinforced by the SUS ring at $z = 0$ during FCM from $B_{\mathrm{ex}} = 9.4$ T ('case C'). The r dependence of $\sigma_\theta^{\,\mathrm{FCM}}$ is in clear contrast to that for the ring bulk reinforced by an aluminum alloy ring shown in figure 6(e) because of the relative relationship of the Young's modulus between the ring materials. The inset of figure 11(b) shows the time step dependence of $\sigma_\theta^{\,\mathrm{FCM}}$(max) for the finite ring bulk with and without the SUS or aluminum alloy ring during the FCM process from 9.4 T, in which the SUS ring restricts the expansion of the ring bulk more effectively than the aluminum alloy ring because of larger Young's modulus.

Figure 11(c) shows the r dependence of the $\sigma_\theta (= \sigma_\theta^{\mathrm{FCM}} + \sigma_\theta^{\mathrm{cool}})$ value of the fourth step at various z-positions in the finite ring bulk reinforced by the SUS ring under FCM process with $B_{\mathrm{ex}} = 9.4$ T ('case C') and combined with cooling from 300 to 50 K. A small positive (tensile) σ_θ value can be observed only at the ring bulk surface ($z = 9.9$ mm), which suggests that the compressive effect of the SUS ring is much more effective, compared to the aluminum alloy ring due to its larger E.

From the present numerical simulation shown in figure 11(c), the actual hoop stress, $\sigma_\theta (= \sigma_\theta^{\mathrm{FCM}} + \sigma_\theta^{\mathrm{cool}})$, of the ring bulk reinforced by the SUS ring during FCM from $B_{\mathrm{ex}} = 9.4$ T was lower than the mechanical strength of REBaCuO bulk [8, 9]. These results suggest that the finite

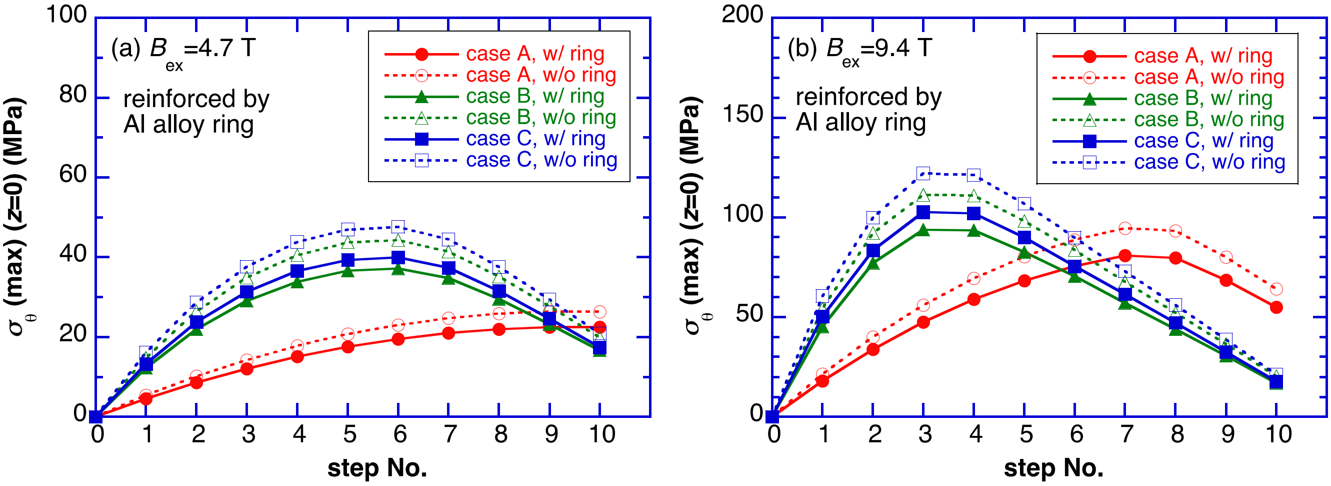

Figure 8. Time step dependence of the maximum electromagnetic hoop stress, $\sigma_\theta{}^{FCM}$(max), in the ring bulk with (w/) and without (w/o) the aluminum alloy ring during FCM from (a) $B_{ex} = 4.7$ T and (b) 9.4 T for all cases.

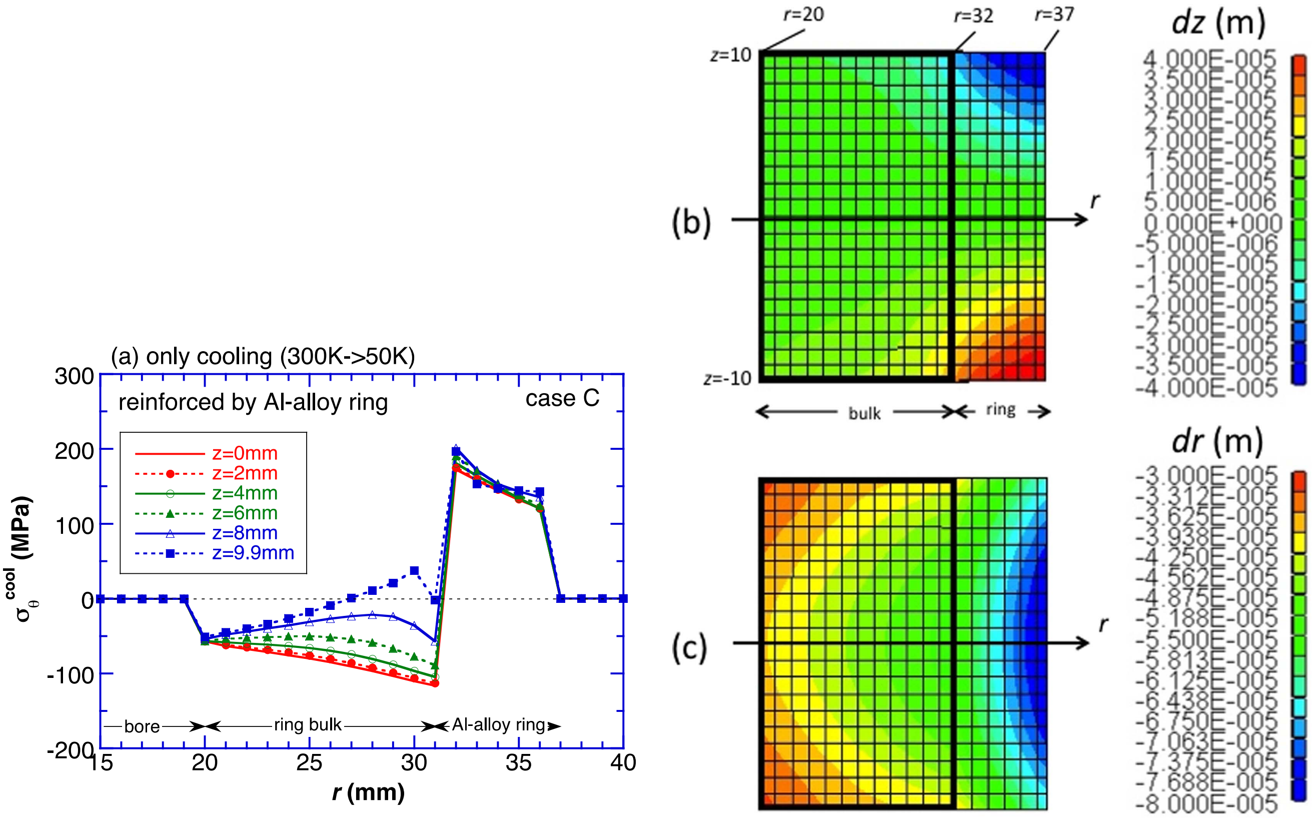

Figure 9. (a) The radius (r) dependence of the thermal hoop stress, $\sigma_\theta{}^{cool}$, for the finite ring bulk reinforced by an aluminum alloy ring for each z-position under cooling from 300 to 50 K. The contour maps of the (b) displacement, dz, along z-direction, and (c) dr, along r-direction under cooling from 300 to 50 K are also shown.

ring bulk would not break during the FCM process, even from $B_{ex} = 9.4$ T. However, actual disk and ring bulks of finite height reinforced by a SUS ring break frequently during FCM under the magnetic fields of several Tesla. Since the REBaCuO bulk superconductor is a composite material, in which the RE_2BaCuO_5 (RE211), Pt and Ag particles are dispersed in the $REBa_2Cu_3O_7$ (RE123) quasi-single crystal matrix with a layered structure, the stress concentration is likely to take place around the so called secondary phases. In addition, the bulk contains a significant number of imperfections such as grain boundaries, crystalline defects, inclusions, voids, and so on. The actual destruction of the REBaCuO bulk during FCM is likely to happen from the mechanically weak points in the bulk material such as voids and crystal imperfections. These imperfections may cause the stress concentration in local regions and may initiate small local cracks. Additionally, micro-cracking along the *ab*-plane formed during post-annealing treatment is a common

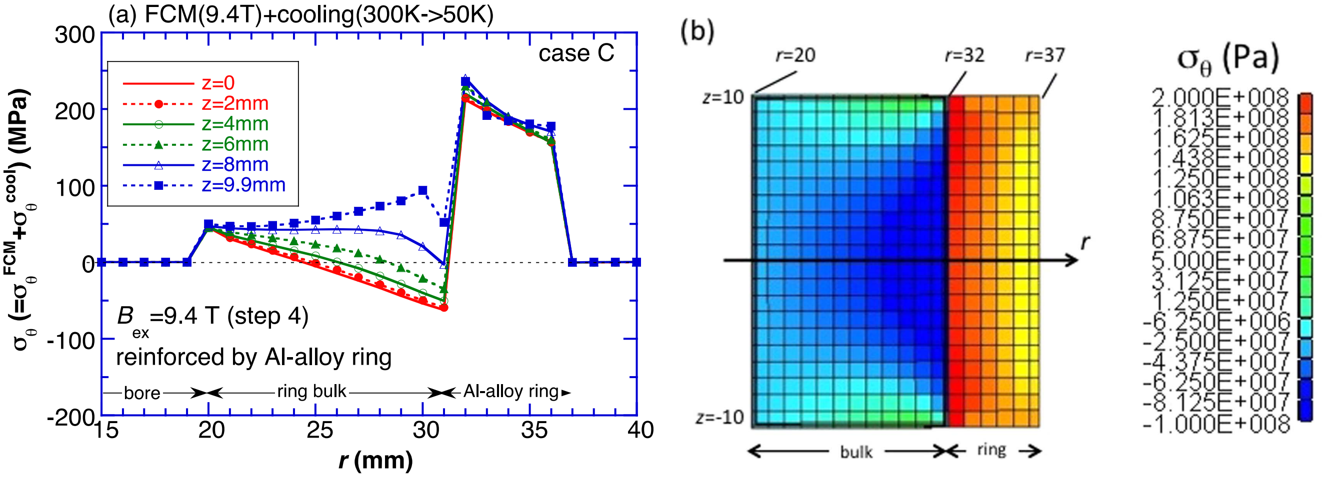

Figure 10. (a) The r dependence of the total hoop stress, $\sigma_\theta (= \sigma_\theta^{\mathrm{FCM}} + \sigma_\theta^{\mathrm{cool}})$, for the finite ring bulk reinforced by an aluminum alloy ring ('case C') at the fourth step of FCM from $B_{\mathrm{ex}} = 9.4$ T under the cooling from 300 K to 50 K. (b) The contour map of the hoop stress, σ_θ, at the fourth step.

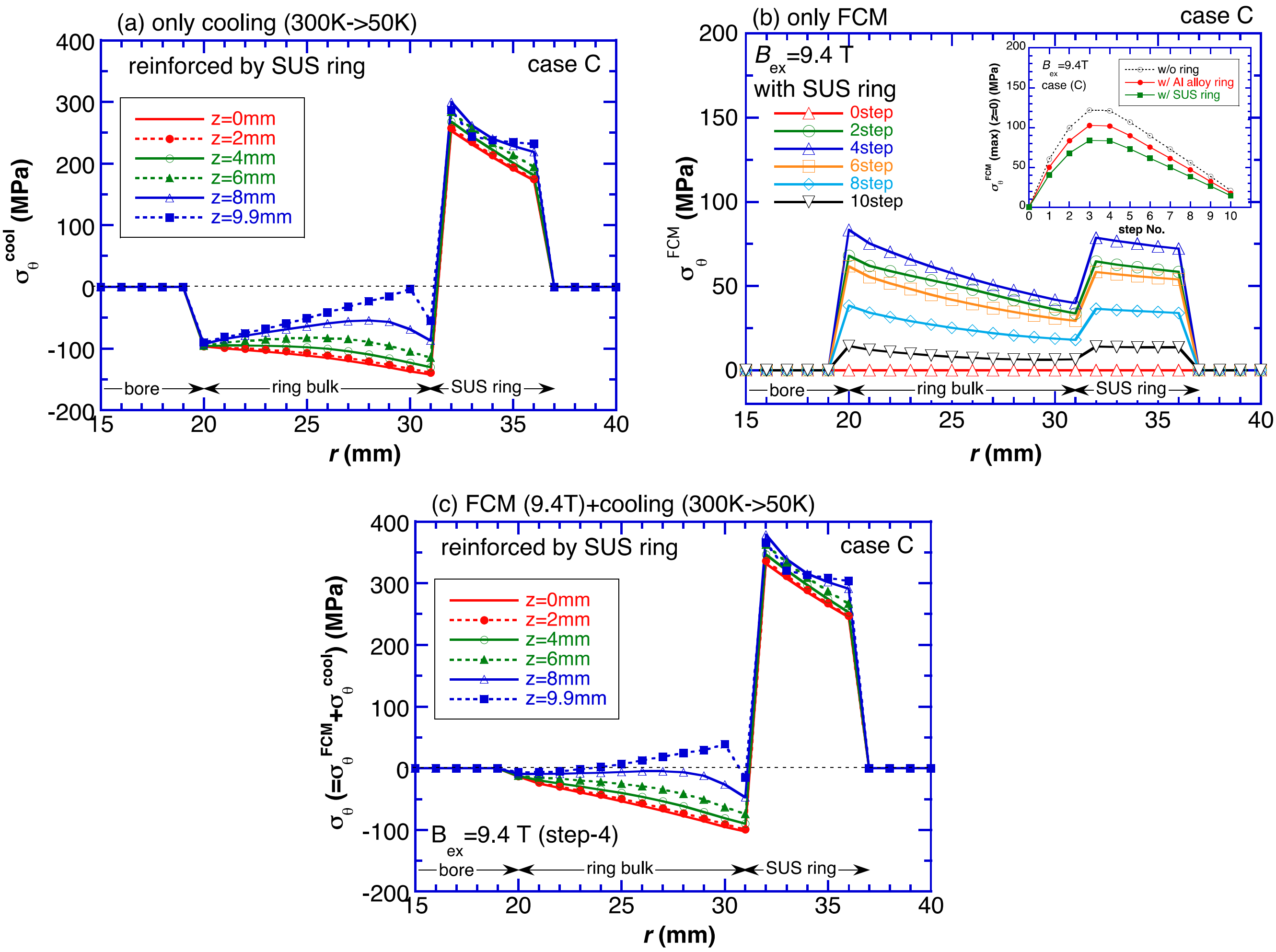

Figure 11. (a) The radius (r) dependence of the thermal hoop stress, $\sigma_\theta^{\mathrm{cool}}$, for the finite ring bulk reinforced by stainless steel (SUS) ring ('case C') under cooling from 300 to 50 K. (b) The r dependence of the electromagnetic hoop stress, $\sigma_\theta^{\mathrm{FCM}}$, for the finite ring bulk reinforced by SUS ring ('case C') during FCM from $B_{\mathrm{ex}} = 9.4$ T without cooling. The inset shows the time step dependence of the $\sigma_\theta^{\mathrm{FCM}}$(max) for the finite ring bulk reinforced by the SUS ring for $B_{\mathrm{ex}} = 9.4$ T, compared to those with and without Al alloy ring. (c) The r dependence of the hoop stress, $\sigma_\theta (= \sigma_\theta^{\mathrm{FCM}} + \sigma_\theta^{\mathrm{cool}})$, for the finite ring bulk reinforced by SUS ring ('case C') during FCM from $B_{\mathrm{ex}} = 9.4$ T under the cooling from 300 to 50 K.

ingredient in the microstructure. These weak points should severely reduce the mechanical strength of the material, as they are the starting points for further cracking under tensile stress. The tiniest hole in the bulk cylinder doubles the tensile hoop stress [13]. As a result, the mechanical stress is concentrated at the weak points, which has a lower mechanical strength, and the bulk would ultimately break. We must consider the numerical simulation of the mechanical properties for the superconductors with such imperfections in the future, and this numerical simulation framework can be easily extended to different superconducting and reinforcing material properties, for various geometries and magnetization processes, such as PFM.

4. Summary

We have performed numerical simulations of the mechanical stresses (hoop stress, σ_θ, and radial stress, σ_r) in a REBaCuO ring bulk of infinite and finite height, reinforced by a metal ring (aluminum alloy or stainless steel), during FCM from $B_{ex} = 4.7$ and 9.4 T using infinite and finite solenoid coils by the FEM. The important analytical results and conclusions are summarized as follows.

(1) The mechanical stresses of the finite ring bulk reinforced by a metal ring during the FCM process have been investigated by FEM for the first time. The electromagnetic hoop stress in the finite ring bulk is larger than that in the infinite ring bulk magnetized by an infinite solenoid coil. The time step dependence of the hoop stress is different for each case. These results suggest that the mechanical stress, especially for the electromagnetic hoop stress, which can be calculated by analytical equations for simple situations, is likely to be underestimated.
(2) The metal ring fitting for the finite ring bulk is confirmed to be effective to reduce the electromagnetic hoop stress during FCM. The reduction effect by the SUS ring is much improved compared with the aluminum alloy ring.
(3) In the actual FCM process, in which a compressive stress is applied to the ring bulk by cooling down to the operating temperature, and then an electromagnetic hoop stress is developed in the ring bulk during FCM, the thermal compressive stress due to the shrink-fit metal ring is effective to reduce the electromagnetic hoop stress and to avoid fracture of the bulk.
(4) However, the thermal hoop stress around the surface of the bulk periphery changes from compressive to tensile stress because of the larger shrink of the metal ring along the axis direction, where the total hoop stress becomes large positively and the bulk is likely to break.
(5) The actual REBaCuO disk or ring bulks of finite height reinforced by a metal ring break frequently under magnetic fields of several Tesla, although the bulk is safe from the simulation results, which assumes homogenous properties. This results from the existence of a large number of imperfections such as grain boundaries, crystalline defects, and voids, at which the mechanical stress is concentrated to the weak points and the bulk breaks finally. We must consider the numerical simulation of the mechanical properties of superconductors including such imperfections in the future.

Acknowledgments

The authors thank Prof. F Nishimura of Iwate University for the valuable discussions of the mechanical stresses. This research is partially supported by a 'Development of Systems and Technologies for Advanced Measurement and Analysis' from Japan Agency for Medical Research and development, AMED, and by JSPS KAKENHI Grant No. 15K04646. Dr Mark Ainslie would like to acknowledge the support of a Royal Academy of Engineering Research Fellowship.

ORCID

M D Ainslie https://orcid.org/0000-0003-0466-3680

References

[1] Durrell J H *et al* 2014 *Supercond. Sci. Technol.* **27** 082001
[2] Tomita M and Murakami M 2003 *Nature* **421** 517–20
[3] Nakamura T, Itoh Y, Yoshikawa M, Oka T and Uzawa J 2007 *Concepts Magn. Reson.* B **31B** 65
[4] Nakamura T, Tamada D, Yanagi Y, Itoh Y, Nemoto T, Utumi H and Kose K 2015 *J. Mag. Reson.* **259** 68–75
[5] Ogawa K, Nakamura T, Terada Y, Kose K and Haishi T 2011 *Appl. Phys. Lett.* **98** 234101
[6] Itoh Y, Yanagi Y and Nakamura T 2017 *J. Cryog. Soc. Japan* **52** 25–32
[7] Fujishiro H, Itoh Y, Yanagi Y and Nakamura T 2015 *Supercond. Sci. Technol.* **28** 095018
[8] Lee D and Salama K 1990 *Japan. J. Appl. Phys.* **29** L2017–9
[9] Fujimoto H and Murakami A 2012 *Supercond. Sci. Technol.* **25** 054017
[10] Miyamoto T, Nagashima K, Sakai N and Murakami M 2000 *Supercond. Sci. Technol.* **13** 816
[11] Mochizuki H, Fujishiro H, Naito T, Itoh Y, Yanagi Y and Nakamura T 2016 *IEEE Trans. Appl. Supercond.* **26** 6800205
[12] Ren Y, Weinstein R, Liu J, Sawh R P and Foster C 1995 *Physica* C **251** 15–26
[13] Johansen T, Wang C, Chen Q Y and Chu W-K 2000 *J. Appl. Phys.* **88** 2730–3
[14] Johansen T 2000 *Supercond. Sci. Technol.* **13** R121–37
[15] Johansen T 1999 *Phys. Rev.* B **60** 9690–703
[16] Huang C, Yong H and Zhou H 2013 *Supercond. Sci. Technol.* **26** 105007
[17] Johansen T H, Chen Q Y and Chu W-K 2001 *Physica* C **349** 201–10
[18] Teshima H, Morita M, Arayashiki T, Naito T and Fujishiro H 2013 *Phys. Procedia* **45** 61–4
[19] Ainslie M D and Fujishiro H 2015 *Supercond. Sci. Technol.* **28** 053002
[20] Ainslie M D, Zhou D, Fujishiro H, Takahashi K, Shi Y-H and Durrell J 2016 *Supercond. Sci. Technol.* **29** 124004
[21] Fujishiro H and Naito T 2010 *Supercond. Sci. Technol.* **23** 105021
[22] Fujishiro H unpublished
[23] Yanagi Y unpublished